Enhanced Vertical Charge Transport in a Semiconducting P3HT Thin Film on Single Layer Graphene

*Vasyl Skrypnychuk, Nicolas Boulanger, Victor Yu, Michael Hilke, Stefan C. B. Mannsfeld, Michael F. Toney, and David R. Barbero**

The crystallization and electrical characterization of the semiconducting polymer poly(3-hexylthiophene) (P3HT) on a single layer graphene sheet is reported. Grazing incidence X-ray diffraction revealed that P3HT crystallizes with a mixture of face-on and edge-on lamellar orientations on graphene compared to mainly edge-on on a silicon substrate. Moreover, whereas ultrathin (10 nm) P3HT films form well oriented face-on and edge-on lamellae, thicker (50 nm) films form a mosaic of lamellae oriented at different angles from the graphene substrate. This mosaic of crystallites with π–π stacking oriented homogeneously at various angles inside the film favors the creation of a continuous pathway of interconnected crystallites, and results in a strong enhancement in vertical charge transport and charge carrier mobility in the thicker P3HT film. These results provide a better understanding of polythiophene crystallization on graphene, and should help the design of more efficient graphene based organic devices by control of the crystallinity of the semiconducting film.

1. Introduction

Graphene, a two dimensional semi-metal made of sp^2 hybridized carbon, is an outstanding material which exhibits high mechanical and chemical stability. Due to its ballistic charge transport and high electron mobility reaching 140 000 $cm^2\ V^{-1}\ s^{-1}$ at room temperature, graphene has been hailed as one of the most exciting new materials for electronic devices.[1,2] The high transparency of single and few layers graphene is advantageous for optoelectronic applications where light must enter the active layer of the device.[3] Recently, devices such as field-effect transistors (FETs), and organic photovoltaics have been produced using graphene.[1,4,5] Moreover, due to its large surface area and highly delocalized electrons, it is expected that graphene can produce efficient charge transfer when in contact with a semiconducting organic material such as P3HT. Strong photoluminescence and fluorescence quenching has been recently reported between graphene and P3HT, indicating electron transfer at the interface between the two materials.[5,6] Already, examples of graphene/P3HT composite devices such as organic memories, photovoltaic devices, and organic field-effect transistors have been demonstrated.[5–9]

Charge transport in conjugated polymers occurs either in the direction of π–π stacking, or along the chain backbone which is the fastest transport direction inside an aggregate. Although processing conditions (e.g. spin speed, solvent) can alter its crystalline orientation, P3HT has a strong tendency to form edge-on lamellae with π–π stacking in the plane of the film on weakly interacting surfaces (e.g. silicon oxide). For this reason, P3HT has been one of the most studied materials for organic based FETs which require high in-plane mobility. [10–13] The strong light absorbance of P3HT in the visible range has also generated a lot of interest as a donor material for photovoltaics (PV). However, in this case the ability to efficiently transport charges vertically (from top to bottom of the film) is a necessary condition. Unfortunately, edge-on orientation does not produce efficient vertical charge transport, and mobility is most often measured in the plane of the film, which does not tell us how efficiently charges can be transported out of plane. Face-on or chain-on orientations would be preferable for vertical charge transport in photovoltaics.[11,14,15] Besides the huge interest generated by both graphene and P3HT for applications, there is still very little known about P3HT crystallization on a graphene surface, and how it affects crystalline orientation and charge transport. A better understanding of this process is therefore of strong interest for both fundamental and applied science.

In this paper, we report the crystallization of highly regioregular P3HT on single layer graphene, and we compare it to a P3HT layer deposited on a silicon wafer with native oxide. The crystalline structure of films with two different thicknesses (10 and 50 nm) was characterized by 2D grazing incidence X-rays diffraction (2D GIXD). The optical and electrical properties of the films were measured by several complementary methods. The films deposited on graphene had a very different distribution of crystallite orientations, and exhibited a much higher degree of π–π stacking perpendicular to the plane of the film, compared to

V. Skrypnychuk, N. Boulanger, Prof. D. R. Barbero
Department of Physics
Umeå University
Umeå 90187, Sweden
E-mail: david.barbero@physics.umu.se
V. Yu, Prof. M. Hilke
Department of Physics
McGill University, Montréal
Québec H3A 2T8, Canada
Prof. S. C. B. Mannsfeld, Dr. M. F. Toney
Stanford Synchrotron Radiation Lightsource
Menlo Park, CA 90187, USA

DOI: 10.1002/adfm.201403418

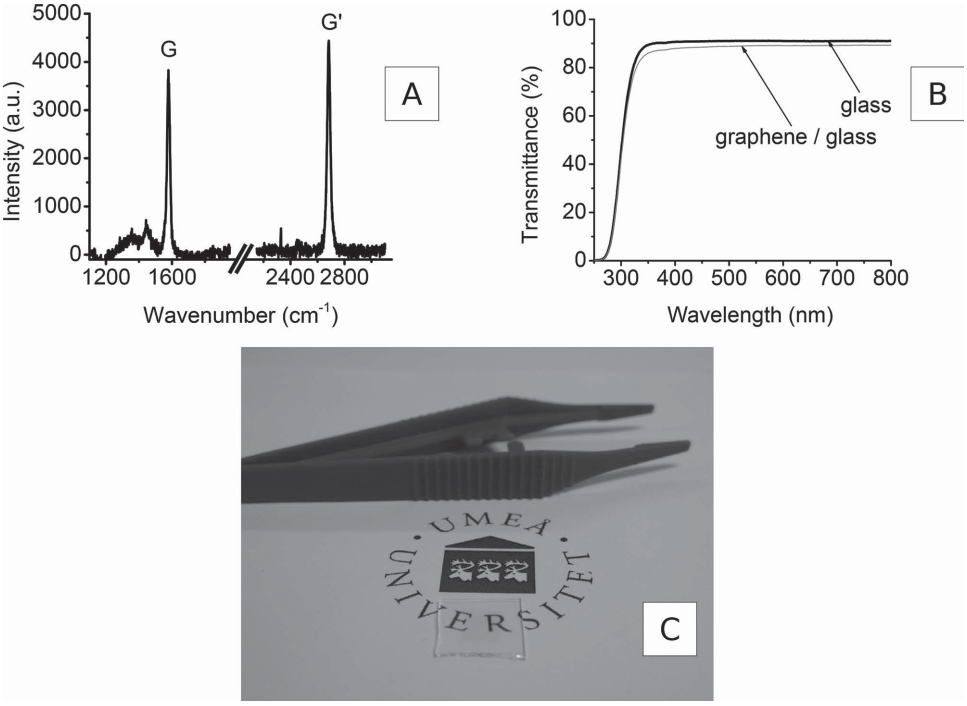

Figure 1. A) Raman spectrum of the graphene layer on silicon where the two characteristic G and G′ peaks are clearly visible. B) UV–vis transmittance of a glass slide and of a graphene/glass sample showing high transmittance and supporting the fact that the graphene is a single layer. C) Graphene layer deposited at the center of a glass sample.

the strong in plane π stacking in films on silicon. Surprisingly, we also observed a clear difference in crystallite orientations between ultrathin (10 nm) and thin (50 nm) films on graphene. A lower amount of face–on lamellae, and a mosaic of π–π orientations, was observed in the 50 nm film on graphene, which resulted in a strong enhancement in vertical charge transport and charge–carrier mobilities. Raman and UV–vis spectroscopy also revealed a slight increase in correlation length and in chain planarity on graphene. These results suggest that graphene could help improve the vertical charge transport, and the efficiency of organic and hybrid light emitting diodes (LEDs) and PVs.

2. Results

Large-area single layer graphene was synthesized on a copper foil by chemical vapor deposition (CVD) using a vertical quartz tube as explained in detail in the Supporting Information.[16] Raman spectroscopy showed full monolayer coverage of the graphene on copper.[17] A free standing graphene layer was then made by etching of the copper foil, and transferred onto a solid substrate (either silicon or glass) by floating in DI water, and dried overnight. Raman spectroscopy of the graphene transferred to silicon (**Figure 1**A) revealed that the characteristic G peak at ≈1580 cm^{-1} and the G′ band at ≈ 2785 cm^{-1} were very sharp and well defined in our samples. The position and the small full width at half maximum (FWHM ≈ 30.8 cm^{-1}) of the G′ band corresponds to single layer graphene.[18]

Figure 1B shows the optical transmittance of a glass slide, and of a layer of graphene deposited on the same glass slide. Glass reflects ≈8% of the incident light which results in a transmittance of ≈92% in the visible spectrum. By contrast the glass/graphene sample transmits slightly less (≈88–90% in the same range of wavelength) due to the slight absorbance of graphene. This can be seen in Figure 1C which shows a monolayer of graphene deposited in the center of a glass substrate, and which appears slightly darker than the glass. The values measured are indeed consistent with the transmittance of a monolayer of graphene reported in the literature.[3] This reflects the high quality and the single layer character of the graphene used in this study.

2.1. Electrical Characterization

Thin films of regioregular P3HT were deposited on silicon and on the graphene/silicon substrate by spin-coating from a dilute solution and annealing at 170 °C. Conductivity and mobility measurements in P3HT films are usually performed in the plane of the film, which is the direction in which the current flows in a FET device. However, the knowledge of the vertical conductivity (across the film thickness) is important for some applications (e.g. photovoltaics), and it is not necessarily the same as in plane. In this study we therefore measured current flow perpendicularly to the film surface, as shown in **Figure 2**A, where a potential difference was applied between the top surface of the film and the conductive substrate, and the resulting current measured across the film thickness. Figure 2B,C reports the current density J (current divided by the surface area of the electrode) as a function of applied voltage U. The measurements were repeated several times for consistency, and the

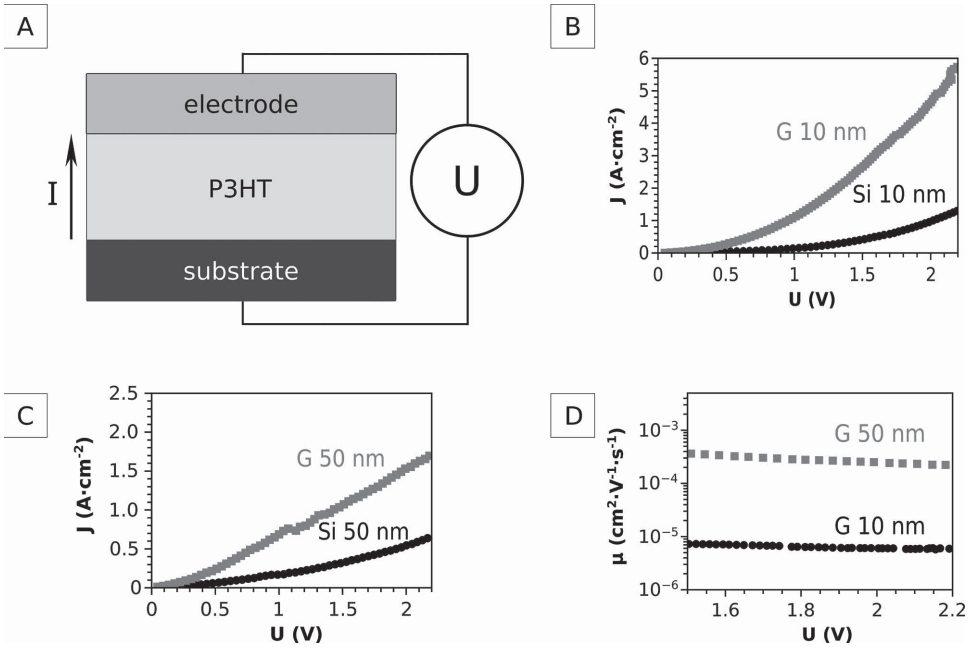

Figure 2. Vertical current density and mobility in the P3HT films. A) Schematics of the measurement where a voltage difference is applied across the film's thickness, and the resulting current is measured in the direction perpendicular to the film. B) Current density–voltage characteristics of 10 nm thick fims, and C) 50 nm thick films on silicon (Si) and graphene (G). D) Room-temperature charge–carrier mobilities in the 10 nm and 50 nm films on graphene.

data points were collapsed onto one curve for each substrate. The conductivity $\sigma\left(\sigma = J \cdot \frac{L}{U}\right)$, where L is the film thickness was measured in the diffusion regime (low voltage). The charge–carrier mobilities μ in the thin P3HT films were extracted by fitting the J-U characteristics with the classical Mott-Gurney equation which is used to describe space–charge–limited current measured in the drift regime (at higher voltages) in organic semiconductors[19]:

$$J = 4\pi^2 \frac{kT}{q} \epsilon \mu \frac{U^2}{L^3} \quad (1)$$

where J is the current density, U the applied voltage, L the sample thickness, ε the dielectric constant of the film, k the Boltzmann constant, T the temperature, and q the elementary charge.

As shown in Figure 2 both P3HT films deposited on graphene were much more conductive than the films on silicon for the same film thickness (either ≈10 nm or ≈50 nm). The P3HT films on silicon reached a maximum conductivity $\sigma \approx 2.2 \times 10^{-4}$ S m^{-1}, which is consistent with previous results obtained in our group, and also as measured by other groups.[20–22] However, when deposited on graphene, the conductivity in the P3HT films increased to $\sigma \approx 4.1 \times 10^{-4}$ S m^{-1} in the 50 nm film. Room temperature vertical mobilities were also higher in the films on graphene and reached $\mu \approx 6.5 \times 10^{-6}$ cm^2 V^{-1} s^{-1} and $\approx 2.8 \times 10^{-4}$ cm^2 V^{-1} s^{-1} in the 10 and 50 nm films respectively, as shown in Figure 2D. The measurements of vertical conductivity and mobility on graphene are the first to be reported, and these are expected to help better design applications where charges must move vertically as opposed to in–plane.

In order to understand the reason for the increased current density and mobility measured in the P3HT films on graphene, we must look at both the energy barrier for charge injection between silicon, graphene and P3HT, and at the crystalline order in the P3HT films. The work functions (WF) of the p-doped silicon substrate (p-Si, WF ≈ –5.1 eV), graphene (WF ≈ –4.6 eV) and P3HT (WF ≈ –4.8 eV) indicate that there is a charge injection barrier between p-Si and graphene.[23,24] Therefore, charge injection is not enhanced by the presence of graphene, unless graphene's WF is modified. Modulation of graphene's work function has been shown by application of a bias, oxygen defects or water adsorption, leading to a reduction in energy barrier.[25,26] This can effectively change the work function of graphene by ≈ 0.2 eV, and enable a slightly better alignment of Fermi levels at the silicon/graphene interface. In agreement with previous studies, hole injection from both p-doped Si and p-doped Si/graphene into P3HT was observed in our experiments.[24] However, based on work functions alone, and since we had not intentionally doped graphene, it is not clear that the graphene layer in our samples helps charge transfer into the organic semiconductor compared to the silicon substrate.[24,27] Moreover, a better energy alignment at interfaces does not explain the strong enhancement in mobilities measured in the 50 nm film compared to the 10 nm on graphene, which have the same energy barriers to charge transport. Another explanation could be that the crystallinity of the P3HT layer is different in the two films. It is indeed well known that crystallinity strongly influences charge transport in organic semiconductors such as P3HT, and we therefore must look in detail at the crystallinity of the P3HT films on both surfaces.

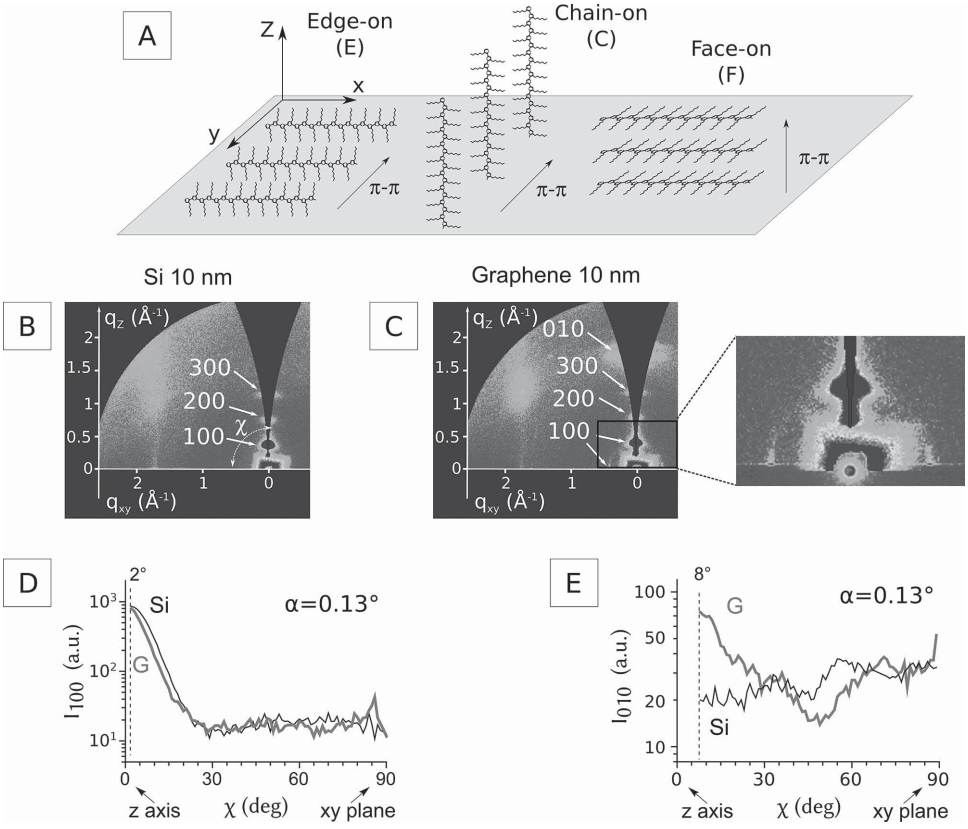

Figure 3. Crystallinity in the 10 nm thick P3HT films at a shallow beam incident angle $\alpha = 0.13°$. A) Possible lamellar orientations in a P3HT film (x–y plane). From left to right: edge-on lamellae with π–π stacking in the plane of the film; chain-on orientation with the P3HT chain backbone vertically oriented along the z axis; face-on lamellae with π–π stacking perpendicular to the plane of the film along the z direction. B,C) 2D grazing incidence diffraction patterns of P3HT on B) silicon, and C) graphene. D,E) Variation of the integrated diffracted intensity as a function of the χ angle for the D) (100), and the E) (010) diffraction. The films were processed and annealed in the same conditions (see text for additional information).

2.2. X-Ray Diffraction and Crystallinity of the Films

Since conjugated polymers are semi-crystalline materials, whose degree of crystallinity and crystallite orientation is critical for charge transport, we performed a study of the crystallinity in these films by the commonly used technique of 2D grazing incidence X-rays diffraction.[28–30] This method gives accurate information about the crystallinity, the crystallites orientation and their coherence length inside the films. The three different possible orientations commonly found in regioregular P3HT films are illustrated in **Figure 3**A. Edge-on where the (100) direction is perpendicular to the substrate and hence both the backbones and the π–π stacking lie in the plane of the film. The second orientation, chain-on, provides the fastest vertical charge transport but is rarely observed with the chains backbones vertically aligned along the z direction.[31] The third possibility is called face-on where π–π stacking is perpendicular to the substrate, which also helps to enable charges to be transported vertically.

The diffraction patterns of 10 nm and 50 nm thin films of highly regioregular P3HT deposited either on silicon or on graphene are shown in Figure 3 and **Figure 4** respectively. These were recorded on a planar area detector which limits slightly the polar angles accessible at large q due to the curvature of the Ewald sphere. This is seen in Figure 3B and Figure 3C where no diffraction is visible along the vertical z axis. On silicon, P3HT films either 10 or 50 nm thick formed clearly visible edge-on lamellae distinguishable by strong diffraction peaks at (100), (200) and (300) along the z axis, as is widely observed in the literature.[14,32–34] The absence of (010) peak near the z axis and of π stacking perpendicular to the substrate on silicon is also in accordance with other studies.[14,35] The ultrathin (10 nm) film showed a strong lamellar alignment in the plane of the film as can be seen by the (h00) diffraction peaks showing little spreading away from the z axis. The 10 nm film deposited on graphene (Figure 3C) also shows strong (h00) alignment along z, but also exhibited a well defined (010) diffraction peak along the z axis, which is characteristic of π–π stacking perpendicular to the plane (face-on in Figure 3A). This result is consistent with binding energy calculations performed between a P3HT chain and a graphene surface, which showed that face-on orientation is favored at the surface of graphene.[36]

One might think that this lamellar arrangement in P3HT would simply extend to thicker films, and show a similar diffraction pattern as for the ultrathin film. However, Figure 4B shows an intense (100) ring in the 50 nm film on graphene, which extends from in-plane ($\chi \approx 90°$) to out-of-plane angles ($\chi \approx 2°$). The (100) diffracted intensity is ≈10 times higher on graphene compared to silicon at high χ angles (Figure 4C). The (010) diffraction on graphene is also more than one order of magnitude more intense than on silicon along the z direction

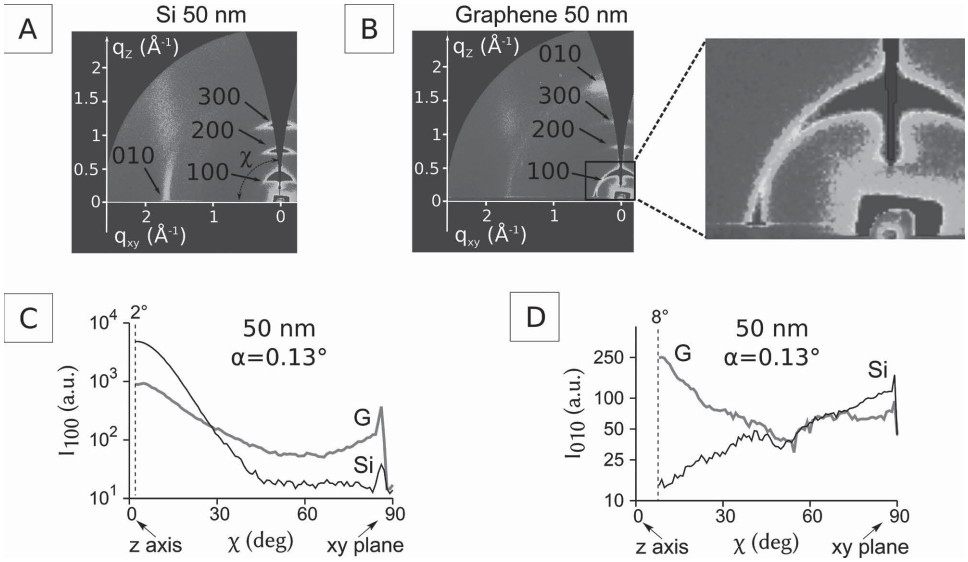

Figure 4. Crystallinity in the 50 nm thick P3HT films at a shallow beam incident angle $\alpha = 0.13°$. A,B) 2D grazing incidence diffraction patterns of P3HT on A) silicon and B) graphene. The magnified view in (B) shows the (100) ring in P3HT on graphene. C,D) Variation of the integrated diffracted intensity as a function of the χ angle on C) silicon and on D) graphene.

(Figure 4D), which is characteristic of π–π stacking perpendicular to the plane (face-on in Figure 3A), instead of in–plane in the film on silicon. The existence of (100) and (010) rings in the 50 nm film on graphene indicates that π–π stacking is oriented uniformly from in-plane to out-of-plane directions inside this film on the graphene substrate. Moreover, the overall amount of face–on lamellae in the 50 nm film is only half of that of the 10 nm (relative to its thickness) on graphene. Since vertical charge transport in P3HT is often associated with face–on lamellae, one would expect the 10 nm film to be much more conductive, which goes against the electrical measurements shown here.

Since charges must be transported across the whole film thickness, it is useful to know how large crystalline domains are in the thicker films, and how charges can be efficiently transported from one ordered aggregate to the next in the vertical direction. The coherence length of the crystalline aggregates was estimated from the FWHM of the (100) diffraction peaks using the Debye-Scherrer equation:

$$l = \frac{K\lambda}{\beta \cos\theta} \tag{2}$$

where l is the coherence length, K is a dimensionless shape factor (typically taken as $K = 0.9$), λ is the X-ray wavelength, β is the peak width at half maximum intensity (FWHM) in radians, θ is the position at the center of the peak.[37–39] This analysis revealed that the out of plane (100) coherence length in the thicker films was ≈20.4 nm on silicon, and ≈12.2 nm on graphene. The out of plane (010) face-on lamellae in P3HT had a coherence length of ≈20.7 nm on graphene. Therefore in the thicker films, several ordered aggregates must be interconnected from top to bottom of the film in order to create a percolated pathway for vertical charge transport. Charges could be transported vertically if several face-on aggregates were connected to each other from top to bottom of the film.

2.3. Crystallinity at the Top of Films

To answer this question, we performed 2D GIXD at a very shallow incident beam angle (0.08°) which probes only the top (≈10 nm) of the thicker P3HT film instead of the whole thickness (50 nm). The 2D diffraction pattern (Figure S3, Supporting Information) showed a similar crystalline orientation in the top layer compared to the whole film on both substrates. Interestingly, the rings in (100) and (010) are also formed in the top layer on the graphene sample, which indicates that the π stacking also exists in all directions in the top layer on graphene. The ratio of diffracted intensities for the two peaks (010) and (100) were calculated to give an idea of the relative proportion of face-on to edge-on lamellae in the top portion of the film and inside the whole film on both substrates. This data is shown in **Table 1** where the intensity ratio I(010)/I(100) was estimated at two χ angles ($\chi \approx 8°$ near out of plane, and $\chi \approx 86°$ in plane). From this analysis, it appears that in the 50 nm film on graphene the proportion of in-plane π stacking is much less than on silicon, and there is a non-negligible amount of out of plane π stacking throughout the film.

Table 1. Intensity ratios I(010)/I(100) in the 50 nm (whole film and top 10 nm), and the 10 nm thick P3HT films. The χ angles are 8° (near out of plane) and 86° (in plane).

Thickness probed	χ	Silicon	Graphene
10 nm	8°	0.02	0.10
10 nm	86°	0.31	0.46
50 nm (Top 10 nm)	8°	0.00	0.10
50 nm (Top 10 nm)	86°	3.28	0.61
50 nm (Whole film)	8°	0.00	0.28
50 nm (Whole film)	86°	3.07	0.25

Remarkably, the intensity ratios are nearly identical (0.25 and 0.28) in the plane and out of plane on graphene, which confirms the even spread of π stacking orientations at all angles observed previously. Moreover, the ultrathin (10 nm) film and the top 10 nm of the thicker film exhibits the same proportion of face–on to edge–on lamellae near z on graphene, but the top 10 nm of the thicker film has ≈ 25 % less face–on lamellae than in the ultrathin 10 nm film.

2.4. Creation of an Interconnected Path for Charge Transport

These results indicate that the strong enhancement in charge carrier mobility in the 50 nm film on graphene is not due to more face-on orientations, but instead it is likely due to a mixture of face-on and edge-on aggregates which creates a continuous pathway (not necessarily the shorter path) for charges to move from top to bottom of the film. It seems reasonable to assume that a high degree of interconnection between crystalline regions, even small aggregates, is a necessary condition for efficient charge transport, as outlined in a recent study.[40] Charges can indeed be transferred from one crystalline region to another by a mechanism of charge hopping across amorphous regions, and charge mobility in P3HT has been shown to only decrease slightly when crossing a small number (5 or less) of grain boundaries.[41] The particular crystalline arrangement of P3HT observed on graphene, which consists of a mosaic of crystalline domains with a large spread of orientations, is likely to favor charge transport vertically across the whole film thickness by forming a continuous pathway of interconnected crystallites and aggregates for charge transport.

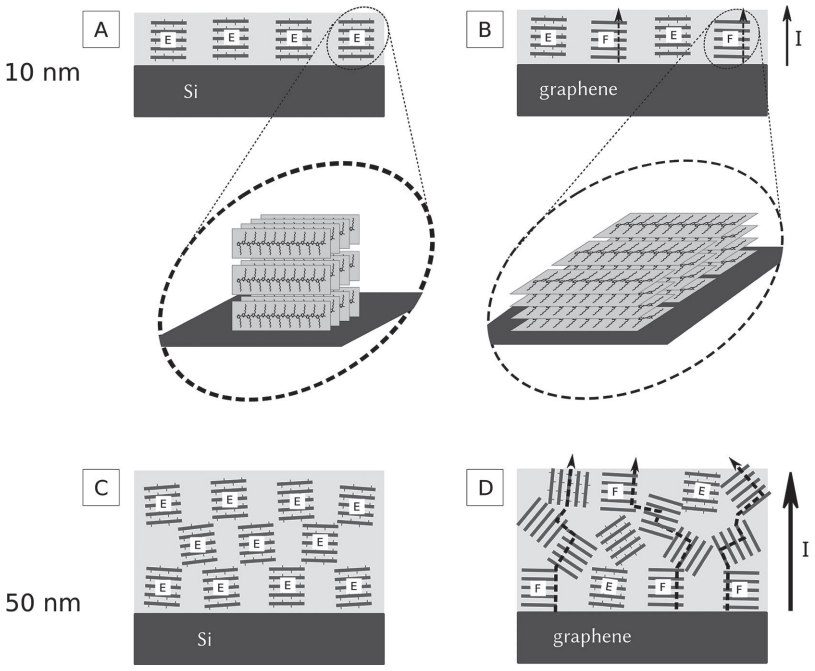

Figure 5. Schematics of charge transport in P3HT on A,C) silicon and B,D) graphene. A,C) P3HT crystalline aggregates on silicon are formed of mainly edge-on lamellae, which results in non-ideal vertical charge transport. B,D) On the graphene surface, aggregates form both edge-on and face-on lamellae. In the 10 nm film, lamellae are well oriented with π–π stacking perpendicular to the plane of the film, whereas in the thicker 50 nm film, a mix of edge-on and face-on lamellae, with various orientations is present. The arrows in (B,D) represent efficient vertical charge transport pathways across the film. The close-ups show the preferential crystalline orientation on both surfaces.

Figure 5 depicts the difference in crystalline orientations, and possible charge transport pathways between the samples. On the silicon surface, P3HT forms mainly edge-on lamellae which are parallel to the surface in both the 10 nm and 50 nm films. On the other hand, on graphene P3HT forms both edge-on and face-on crystallites, which help with vertical charge transport compared to only edge-on or face-on. The strong ordering of crystallites (sharp peaks along z) in the 10 nm film is likely due to strong π interactions with the substrate, and to confinement effects since the crystallite size is almost the same as film thickness. However, in the 50 nm film on graphene, several crystallites are necessary to bridge the bottom to the top of the film. The crystallites next to the substrate are likely well ordered with face–on and edge–on oriented along z due to strong interactions with the graphene layer, as shown in the 10 nm film. However, as the thickness increases there is less interaction with the substrate, and crystallites can adopt different orientations, giving rise to a spread of orientations. This spread creates an interconnected pathway for charge transport across the film along the π–π stacking (and possibly also along the chain backbone) from 0 and 90° angles. From these results, it appears that graphene is a material of choice for obtaining crystalline orientations that favor vertical charge transport in P3HT, and it might help improve the efficiency of organic and hybrid OLED and OPV devices.

3. Conclusion

In conclusion, we have shown that graphene induces the crystallization of both face-on and edge-on lamellae on its surface. In very thin layers (10 nm) the lamellae are mostly parallel to the plane, whereas in thicker (50 nm) films, a large spread of crystalline orientations is formed. This particular crystalline mosaic with π–π stacking oriented homogeneously at various angles inside the film favors the creation of a continuous pathway of interconnected crystallites for charge transport. Conductivity measurements showed a strong increase in mobility and charge transport in P3HT when deposited on graphene.

4. Experimental Section

Materials: Poly-3-hexylthiophene (P3HT) (98% RR, Mw = 32 kD) was purchased from American Dye Source Inc. Single layer graphene was produced by CVD on a copper foil and subsequently transferred to a solid substrate (silicon or glass). Details of the synthesis and transfer procedure of graphene, and other materials used can be found in the Supporting Information.

Sample Preparation: The P3HT films were prepared as described in the Supporting Information. The films were then annealed in inert nitrogen atmosphere at 170 °C for 15 min, followed by slow cooling (≈1 °C·min^{-1}) to room temperature.

Sample Characterization: The samples were characterized by AFM (Veeco Multimode) for the determination of film thickness, and by Raman (Renishaw InVia) and UV–vis spectroscopy (Perkin-Elmer) for determination of their optical and physical properties. Crystallinity of the P3HT films was measured by 2D Grazing-incidence X-ray diffraction carried out at the Stanford Synchrotron Radiation Lightsource (SSRL) (Menlo Park, CA, USA). See Supporting Information for more details.

Supporting Information

Supporting Information is available online from the Wiley Online Library or from the author.

Acknowledgements

Portions of this research were carried out at the Stanford Synchrotron Radiation Lightsource, a Directorate of SLAC National Accelerator Laboratory and an Office of Science User Facility operated for the US Department of Energy Office of Science by Stanford University. Some sample preparation was performed at MyFab (Ångström Laboratory) at Uppsala University. The authors thank the Baltic Foundation, MyFab and the Kempe Foundation for financial support. D.R.B. also thanks a Young Researcher Career Award from the Faculty of Science and Technology at Umeå University.

Received: September 30, 2014
Published online: November 6, 2014

[1] K. S. Novoselov, A. K. Geim, S. V. Morozov, D. Jiang, Y. Zhang, S. V. Dubonos, I. V. Grigorieva, A. A. Firsov, *Science* **2004**, *306*, 666.
[2] L. Wang, I. Meric, P. Y. Huang, Q. Gao, Y. Gao, H. Tran, T. Taniguchi, K. Watanabe, L. M. Campos, D. A. Muller, J. Guo, P. Kim, J. Hone, K. L. Shepard, C. R. Dean, *Science* **2013**, *342*, 614.
[3] F. Bonaccorso, Z. Sun, T. Hasan, A. C. Ferrari, *Nat. Photonics* **2010**, *4*, 611.
[4] B. Obradovic, R. Kotlyar, F. Heinz, P. Matagne, T. Rakshit, M. D. Giles, M. A. Stettler, D. E. Nikonov, *Appl. Phys. Lett.* **2006**, *88*, 142102.
[5] Z. Liu, Q. Liu, Y. Huang, Y. Ma, S. Yin, X. Zhang, W. Sun, Y. Chen, *Adv. Mater.* **2008**, *20*, 3924.
[6] L. Zhang, Y. Li, J. Shi, G. Shi, S. Cao, *Mater. Chem. Phys.* **2013**, *142*, 626.
[7] Y. C. Lai, Y. X. Wang, Y. C. Huang, T. Y. Lin, Y. P. Hsieh, Y. J. Yang, Y. F. Chen, *Adv. Funct. Mater.* **2013**, *24*, 1430.
[8] Y. Wu, X. Zhang, J. Jie, C. Xie, X. Zhang, B. Sun, Y. Wang, P. Gao, *J. Phys. Chem. C* **2013**, *117*, 11968.
[9] J. Huang, D. R. Hines, B. J. Jung, M. S. Bronsgeest, A. Tunnell, V. Ballarotto, H. E. Katz, M. S. Fuhrer, E. D. Williams, J. Cumings, *Org. Electron.* **2011**, *12*, 1471.
[10] G. Wang, J. Swensen, D. Moses, A. J. Heeger, *J. Appl. Phys.* **2003**, *93*, 6137.
[11] H. Yang, T. Shin, L. Yang, K. Cho, C. Ryu, Z. Bao, *Adv. Funct. Mater.* **2005**, *15*, 671.
[12] M. Surin, P. Leclère, R. Lazzaroni, J. D. Yuen, G. Wang, D. Moses, A. J. Heeger, S. Cho, K. Lee, *J. Appl. Phys.* **2006**, *100*, 033712.
[13] D. Gargi, R. J. Kline, D. M. DeLongchamp, D. A. Fischer, M. F. Toney, B. T. O'Connor, *J. Phys. Chem. C* **2013**, *117*, 17421.
[14] L. H. Jimison, S. Himmelberger, D. T. Duong, J. Rivnay, M. F. Toney, A. Salleo, *J. Polym. Sci., Part B: Polym. Phys.* **2013**, *51*, 611.
[15] W. Porzio, G. Scavia, L. Barba, G. Arrighetti, S. Milita, *Eur. Polym. J.* **2011**, *47*, 273.
[16] D. R. Cooper, B. D'Anjou, N. Ghattamaneni, B. Harack, M. Hilke, A. Horth, N. Majlis, M. Massicotte, L. Vandsburger, E. Whiteway, V. Yu, *ISRN Condens. Matter Phys.* **2012**, *2012*, 501686.
[17] V. Yu, E. Whiteway, J. Maassen, M. Hilke, *Phys. Rev. B* **2011**, *84*, 205407.
[18] A. C. Ferrari, J. C. Meyer, V. Scardaci, C. Casiraghi, M. Lazzeri, F. Mauri, S. Piscanec, D. Jiang, K. S. Novoselov, S. Roth, A. K. Geim, *Phys. Rev. Lett.* **2006**, *97*, 187401.
[19] N. F. Mott, R. W. Gurney, *Electronic Processes in Ionic Crystals* Dover Publications, New York, **1964**.
[20] D. R. Barbero, N. Boulanger, M. Ramstedt, J. Yu, *Adv. Mater.* **2014**, *26*, 3111.
[21] J. Obrzut, K. A. Page, *Phys. Rev. B* **2009**, *80*, 195211.
[22] M. Osaka, H. Benten, L. T. Lee, H. Ohkita, S. Ito, *Polymer* **2013**, *54*, 3443.
[23] A. Novikov, *Solid-State Electron.* **2010**, *54*, 8.
[24] R. Yan, Q. Zhang, W. Li, I. Calizo, T. Shen, C. A. Richter, A. R. Hight-Walker, X. Liang, A. Seabaugh, D. Jena, H. Grace Xing, D. J. Gundlach, N. V. Nguyen, *Appl. Phys. Lett.* **2012**, *101*, 022105.
[25] H. Yang, J. Heo, S. Park, H. J. Song, D. H. Seo, K. E. Byun, P. Kim, I. Yoo, H. J. Chung, K. Kim, *Science* **2012**, *336*, 1140.
[26] M. G. Lemaitre, E. P. Donoghue, M. A. McCarthy, B. Liu, S. Tongay, B. Gila, P. Kumar, R. K. Singh, B. R. Appleton, A. G. Rinzler, *ACS Nano* **2012**, *6*, 9095.
[27] B. R. Matis, J. S. Burgess, F. A. Bulat, A. L. Friedman, B. H. Houston, J. W. Baldwin, *ACS Nano* **2012**, *6*, 17.
[28] J. Rivnay, S. C. B. Mannsfeld, C. E. Miller, A. Salleo, M. F. Toney, *Chem. Rev.* **2012**, *112*, 5488.
[29] D. M. DeLongchamp, R. J. Kline, D. A. Fischer, L. J. Richter, M. F. Toney, *Adv. Mater.* **2011**, *23*, 319.
[30] J. L. Baker, L. H. Jimison, S. Mannsfeld, S. Volkman, S. Yin, V. Subramanian, A. Salleo, A. P. Alivisatos, M. F. Toney, *Langmuir* **2010**, *26*, 9146.
[31] Y. K. Lan, C. I. Huang, *J. Phys. Chem. B* **2008**, *112*, 14857.
[32] T. Salammal Shabi, S. Grigorian, M. Brinkmann, U. Pietsch, N. Koenen, N. Kayunkid, U. Scherf, *J. Appl. Polym. Sci.* **2012**, *125*, 2335.
[33] G. Scavia, W. Porzio, S. Destri, L. Barba, G. Arrighetti, S. Milita, L. Fumagalli, D. Natali, M. Sampietro, *Surf. Sci.* **2008**, *602*, 3106.
[34] E. Verploegen, R. Mondal, C. J. Bettinger, S. Sok, M. F. Toney, Z. Bao, *Adv. Funct. Mater.* **2010**, *20*, 3519.
[35] D. M. DeLongchamp, R. J. Kline, Y. Jung, E. K. Lin, D. A. Fischer, D. J. Gundlach, S. K. Cotts, A. J. Moad, L. J. Richter, M. F. Toney, M. Heeney, I. McCulloch, *Macromolecules* **2008**, *41*, 5709.
[36] D. H. Kim, H. S. Lee, H. J. Shin, Y. S. Bae, K. H. Lee, S. W. Kim, D. Choi, J. Y. Choi, *Soft Matter* **2013**, *9*, 5355.
[37] A. Salleo, R. J. Kline, D. M. DeLongchamp, M. L. Chabinyc, *Adv. Mater.* **2010**, *22*, 3812.
[38] J. Rivnay, R. Noriega, R. J. Kline, A. Salleo, M. F. Toney, *Phys. Rev. B* **2011**, *84*, 045203.
[39] W. Chen, M. P. Nikiforov, S. B. Darling, *Energy Environ. Sci.* **2012**, *5*, 8045.
[40] R. Noriega, J. Rivnay, K. Vandewal, F. P. V. Koch, N. Stingelin, P. Smith, M. F. Toney, A. Salleo, *Nat. Mater.* **2013**, *12*, 1038.
[41] E. J. W. Crossland, K. Tremel, F. Fischer, K. Rahimi, G. Reiter, U. Steiner, S. Ludwigs, *Adv. Mater.* **2012**, *24*, 839.